



Migration of Water Molecules in the Permanently Shaded Areas of Polar Areas of Mercury

E. A. Feoktistova¹ · A. Y. Zharkova^{1,2} · A. A. Kokhanov² · Zh F. Rodionova¹

Received: 21 September 2020 / Accepted: 24 July 2021 / Published online: 28 August 2021
© The Author(s), under exclusive licence to Springer Nature B.V. 2021

Abstract

Radar observations of the surface of Mercury had revealed areas with bright reflective properties in both polar regions of the planet. It was suggested that such areas contain depositions of volatile compounds, including water. In this paper, we investigated migration of water molecules to the permanently shaded areas, located in the impact crater in the polar regions of Mercury. To simulate the migration of water molecules in the exosphere of Mercury, we used the Monte Carlo method. To estimate the proportion of water molecules falling into cold traps in the polar regions of Mercury, we estimated the area of such regions. We found that the area of permanently shaded areas near the north pole of the planet reaches 23,300 km², and in the area of the south pole—45,500 km². Most of the water molecules (~92%) will be destroyed as a result of photolysis, and ~7.5% of them will be destroyed while they are on the planet's surface between hops. The fraction of water molecules that left the planet's exosphere as a result of reaching the escape velocity is only 0.3%. The fraction of water molecules trapped in permanently shaded areas in the polar regions of Mercury reaches 7.8% of the total number of particles participating in the simulation. Only 2.2% of them can be trapped in cold traps in the North Pole region and 5.6% in the South Pole region.

Keywords Mercury · Polar region · Craters · Volatiles

1 Introduction

For the first time, areas with anomalous radio-reflective properties have been discovered on the polar regions of Mercury during surface studies via telescopes of Arecibo and Goldstone observatories in 1991–1992 (Harmon and Slade 1992; Harmon et al. 2001). Mercury surface studies continued through telescopes Goldstone and Arecibo (Harmon et al. 2011). As a result of these studies, the number of discovered regions with anomalous

✉ E. A. Feoktistova
Hrulis@yandex.ru

¹ Sternberg State Astronomical Institute, M.V. Lomonosov Moscow State University, Universitetsky prospekt 13, Moscow 119234, Russian Federation

² Moscow State University of Geodesy and Cartography (MIIGAik), Gorokhovskiy pereulok 4, Moscow 105064, Russian Federation

reflective characteristics in polar regions of the planet have been significantly increased (Chabot et al. 2018). Such areas were discovered in relief depressions, primarily in impact craters. Several of these regions had the form of a crescent and were located on impact crater's sides that were situated opposite to the pole. This fact allowed to assume that these regions comprise accumulations of volatile compounds that were stored in the permanently shaded areas of impact craters—"cold traps"—for a long time. The MESSENGER (Mercury Surface, Space Environment, GEOchemistry and Ranging) (2008–2015) probe was the first spacecraft to explore Mercury since 1974. Due to specifics of spacecraft's orbit, the obtained data mainly covered Mercury's North pole. Among other things, these data confirmed the existence of regions with increased reflectivity in craters, located in polar regions of the planet (Neumann et al. 2013). The data from the MESSENGER probe neutron spectrometer indicate that the deposits of volatile compounds in the North Pole region contain tens of centimeter thick hydrogen-enriched layer (Lawrence et al. 2013). This confirmed the assumptions that these formations may be deposits of volatile compounds, including water ice. In (Lawrence et al. 2013), it was suggested that the soil of these areas may consist of several layers, with a second layer located under a less hydrogen-containing layer 10–30 cm thick, the thickness of which is estimated from 50 to 20 m. The combination of the radar data and the neutron spectrometer of the MESSENGER probe suggests a layer of almost pure water under the regolith layer with a hydrogen fraction corresponding to 25% water equivalent content. In this case, the lower layer can be a mixture, the main components of which are water and organic compounds (Paige et al. 2012). The assumptions that the main component of the soil of "cold traps" on Mercury is water ice are also confirmed by the data of long-term ground-based radio observations (Harmon et al. 2011; Cremonese et al. 2010).

2 Sources of the Volatile Compounds

The volatile compounds in the polar regions of Mercury could be accumulated as a result of the endogenous activity such as subsoil degassing and volcanic activity on the planet's surface. The main volcanic activity on Mercury took place in past (Thomas et al. 2014; Byrne et al. 2016): the epoch of volcanic volcanism dates back to about 4.1 billion years ago, and the period of explosive volcanism ended about 1 billion years ago. Despite the fact that it is believed that currently Mercury is not active, the volcanic processes could be the sources of water, as well as of the other compounds (Fegley 1991). Exogenous sources are the solar wind and meteorites, asteroids, and comets. Solar wind protons can create molecules of water and hydroxyl during interactions with Mercury's regolith (Jones et al. 2020). Impacting asteroids and comets may deliver such compounds such H_2O , CO , CO_2 and others. In addition to water, the composition of comets includes a number of compounds, such as, for example, CO , CO_2 , H_2CO , CH_3OH , CH_4 , C_2H_6 , NH_3 , H_2S , and others (Zhang and Paige 2009). Discovery of volatile compounds accumulation during the impact experiment executed through LCROSS spacecraft on the shadowed region of the Cabeus crater on the Moon also adds to the possibility of volatile compounds accumulation in the "cold traps" in the polar regions of the airless bodies of the Solar System (Colaprete et al. 2010; Gladstone et al. 2010). According to different estimations, the fraction of volatile compounds that stay on the planet during and after Mercury's collisions with comets is 1.5 to 7.1% (Moses et al. 1999) or up to 10% (Pierazzo and Chyba 1999). Meteoroids can be another source of matter delivered to planets. Nesvorný et al. (2010) found that up to

85% of the matter coming to Earth from space is micrometeorites. According to (Nesvorniy et al., 2010), comets are the sources of about 90% of such micrometeorites, while asteroids are only 10%.

3 The Model of Movement of Water Molecules

The migration of volatile compounds in the exosphere of the Solar System celestial bodies has been the subject of numerous studies (Wurz and Lammer 2003; Moores 2015; Schorghofer 2015). We have modeled the water molecules motion in the exosphere of the planet by the Monte-Carlo method. Numerous works, including (Moores 2015), choose the noon at the equator as the place and the start time for all molecules' movement. In our work, the initial location and the start time were mostly random, with one restriction: molecular movement always started at the sunlit side of the planet—the exact moment was defined through the longitude of the subsolar point, selected randomly. The water molecule on the surface can be destroyed as a result of photolysis or can evaporate as a result of thermal desorption. The residence time of a molecule on the surface can be described by the formula:–

$$\tau_{\text{res}} = 1/\tau \quad (1)$$

where $\tau = 1/\tau_{\text{th}} + 1/\tau_{\text{phot}}$ (τ_{th} –time of thermal desorption of a molecule; τ_{phot} –time of destruction of a molecule as a result of photolysis ($1.1 * 10^4$ s (Huebner et al. 1992)). The thermal desorption time depends on the surface temperature at the location of the molecule:

$$\tau_{\text{th}} = \tau_0 \exp(E_{\text{act}}/kT) \quad (2)$$

where τ_0 –vibrational period of an H₂O molecule in a potential well, E_{act} –desorption energy, T –surface temperature. For the physical desorption $\tau_0 = 10^{-12}$ s, $E_{\text{act}} = 0.41$ eV, for chemisorption these values are $\tau_0 = 1.2 * 10^{-9}$ s, $E_{\text{act}} = 0.72$ eV respectively (Grumpe et al. 2019). Velocity of emission of molecules v_0 was determined by the Maxwell–Boltzmann distribution as a function of surface temperature, similar to (Schorghofer 2015):

$$f(v_0) = 4\pi v_0^2 \sqrt{(m/2\pi kT)^3} e^{-mv_0^2/2kT} \quad (3)$$

where m is the mass of the water molecules ($m = 3 * 10^{-26}$ g), k is the Boltzmann constant ($k = 1.38 * 10^{-23}$ J/K). If the velocity of the molecule was equal to or exceeded the escape velocity for Mercury ($v_{\text{esc}} = 4251$ m/s), the molecule was considered out of consideration.

The temperature of the surface in the region where the molecules were situated was calculated, using the position of the Sun and the local time. Due to the fact Mercury rotates twice around the Sun during a solar day, the model comprised the change of the distance between the planet and the Sun and the changes of its angular diameter during the daily orbital movement. After the sunset, the surface temperature drops very quickly and stays low (~100 K) until the sunrise. Reasoning from this fact, we suggested that, after the “jump” on the “night” side of the planet, water molecules stay there until sunrise.

The direction of movement of the molecule was determined in the horizontal coordinate system: azimuth j and angle Θ —between the molecular velocity vector and the horizontal plane. The values of the j and Θ angles were determined randomly. During the calculation of the particle's flying up angle, the roughness of the surface has not been considered. In (Butler 1997), the roughness of the surface was accepted as the same for Mercury and for

the Moon and equaled 5° on average. We assumed that if the particle emergent angle was less than 5° , the particle was considered not to take off at the moment and the emergent simulation continued until the value of the emergent angle exceeded 5° .

The molecules that flew up were migrating in the planet's exosphere through ballistic trajectories. The trajectory and the duration of each molecular jump were calculated as they have been in (Wurz and Lammer 2003). To do this, the molecule's flight path was divided into 100 intervals, and each of them considered the change of the speed and of the flight path angle during upward and downward movements. The hop height of the molecule was determined as:

$$h = Rv_h^2 / (2Rg_0 - v_h^2) \quad (4)$$

where R —radius of Mercury (2439 km), $v_h = v_0 \sin \Theta$, $g_0 = 3.72 \text{ m/s}^2$ —the surface gravity.

At each height interval, the molecular velocity was determined as:

$$v_{hi} = v_{hi-1} \pm g_i t_i \quad (5)$$

where v_{hi-1} —molecule velocity at the previous ($i-1$) height interval, g_i —gravity at the h_i distance from the planet surface: $g_i = g_0(R / (R + h_i))^2$ (Butler 1997). The “+” sign in formula (5) was used for an upward movement and a “-” sign—for a downward movement.

The flight period was calculated as a sum for each region of the trajectory. During the flight, molecules could be destroyed during photolysis. The probability of destruction of a molecule in flight as a result of photolysis is defined as (Prem et al. 2015):

$$P = 1 - e^{-t/\tau_{\text{phot}}} \quad (6)$$

where t is the “jump” time of the molecule in the exosphere, τ_{phot} is the photolysis time ($1.1 * 10^4 \text{ s}$) (Huebner et al. 1992). If the destruction of the molecule as a result of photolysis during the flight did not occur and if its speed was lower than escape velocity, it went down back on the surface. The coordinates of the landing location were calculated according to (Butler 1997) and took account of the rotation of the planet on its axis and around the Sun during a particle's flight time. If the particle landed on the “night” side of the planet, it was considered to remain in its location until sunrise, and period of time when the particle stays on the surface included the time of the “night” left until the sunrise lit up “night” side.

4 The Evaluation Model of Molecules that Accumulated in the Polar Regions of the Planet

In several studies (Butler 1997; Moores 2015), molecules that appear in the permanently shadowed regions of polar areas of the planet were defined as particles that landed on the surface under the angle higher than 85° . In this paper, we attempted to get more details about the probability of water molecules getting into the permanently shadowed areas of craters located in the polar regions of Mercury. We used the data of MESSENGER, particularly, the global digital elevation model (DEM) with the resolution 665 m/pixel (Becker et al. 2016), obtained through photogrammetric methods, to evaluate the fraction of permanently shadowed areas of the surface in polar regions of the planet. Despite the fact that some studies (Chabot et al. 2018) showed that constantly shaded areas of the surface can exist not only in impact craters, but in other ridged areas in polar regions of the planet, the

main accumulations of volatile compounds on the Mercury have been discovered inside impact craters (Harmon and Perillat, 2001; Neumann et al. 2013). Not every crater contains permanently shadowed areas: if the crater walls' slope angle is lower than the solar angle for the point, there will not be permanently shadowed areas inside. Permanently shadowed areas exist in relatively young craters with a rim that is not destroyed or smoothed. According to the classification, developed in Sternberg Astronomical Institute (SAI) (Sitnikov et al. 2005), such craters can be defined as craters belong to preservation class 1–3.

To describe the craters in SAI catalog an addition to the coordinates and diameter of the crater, nine morphological features are used. Each of these features includes a number of sub-features: degree of rim degradation (5 classes: from 1 (high preserved) to 5 (wholly degraded rim)); terraces and faults; character of rim; character of central feature; chains of craters and fissures; character of the crater floor; lava on the crater floor; presence of ray system; local terrain.

We calculated the presence of permanently shadowed areas in impact craters of 1–3 degree of preservation on both polar regions of the planet. We investigated craters with the diameter equal or higher than 10 km only, since according to (Vasavada et al. 1999) in craters of a smaller diameters, irradiation from illuminated walls heats the permanently shadowed areas so much, that the temperature does not allow gathering of water ice and other volatile compounds to accumulate for a long time. To do this we used the New global catalog of Mercury's craters, created by SAI and Moscow State University of Geodesy and Cartography (Feoktistova et al. 2020). This catalog contains information on the morphological characteristics of about 21,000 craters over ten kilometers in diameter and various morphometric parameters for craters of all diameters. Among them: depth, the ratio of depth to diameter and steepness of craters' slopes. Currently the catalog is in the development state. According to our data, the polar regions of the planet ($|\varphi| \geq \pm 60^\circ$, where φ is the latitude) contain 1408 craters with the diameters of ≥ 10 km, where 658 craters have 1–3 preservation degree by SAI classification. 261 of such craters are situated in the north polar region of Mercury, and 397 are in the South polar areas. To evaluate the areas of constantly shadowed regions inside of these craters, we used data about morphometric parameters of Mercury's craters, such as depth, walls' slope angle, and the diameter of flat bottoms (for complex craters) that is consistent with craters' preservation degree, according to (Pike 1988). Complex craters were modeled by truncated cones with the corresponding parameters, and simple craters by a sphere segment: the surface of the inner slopes of the crater was divided into 3600 elements: 10 levels in height and 360 parts around the rim circle. In complex craters, their flat bottoms were divided into 3600 elements using the same method. In that case, the inner surface of such craters was broken down to 7200 elements. If crater had a central height (such as a hill or a peak), its form was also modeled using morphometric formulas from (Pike 1988) (Fig. 2). For each element of the inner craters' surfaces we defined the angle of altitude of other visible elements from the chosen point of the surface and calculated their effect on the solar illumination for this element during the day. If the surface elements stayed shadowed during the entire period, it was considered as permanently shadowed.

Figure 1 shows a comparison of the latitudinal profile of the crater (85.2° S, 13.6° W), which contains the region with anomalous reflective properties of V3, which is supposed to be deposits of volatile compounds, and the profile of this crater constructed according to the model (Pike 1988). As it is presented in the image, the results of this crater's morphometric parameters modeling via (Pike 1988) are consistent with its measured parameters. Despite the fact that such modeling does not always show accurate parameters of the crater, it allows to generally evaluate constantly shadowed areas in the given regions. A simulation

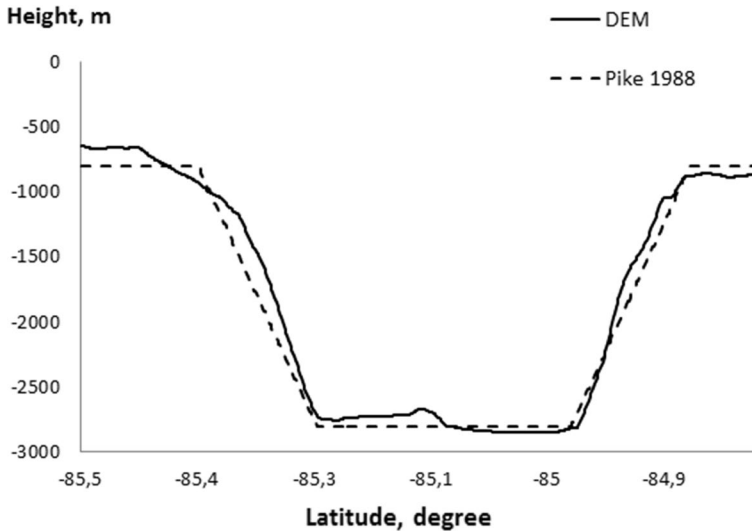


Fig. 1 The east–west line of the crater (85.2° S, 13.6° W) modeled using the global Mercury DEM data (Becker et al. 2016) and the profile of this crater by model (Pike 1988). In the crater (85.2° S, 13.6° W), the area V3 is located, that contains the accumulation of volatile compounds (Harmon and Slade, 1992)

of the inner shape of the Hurley crater (87.4° S, 7° W), located in the region of the south pole of Mercury and containing the formation with anomalous reflective properties (radar bright feature) U, is shown in Fig. 2. On the slope of the Hurley crater its satellite crater is shown, in which a radar-bright feature was also found.

5 Results

According to the obtained results, in Mercury’s North Pole only 84 craters with a diameter ≥ 10 km contain permanently shadowed regions. The South Pole of the planet contains more such craters—108. The area of permanently shadowed regions on the Mercury’s North Pole ($\varphi \geq 60^\circ$) is $\sim 23,300$ km², according to our data, and it is 45500 km² (Table.1) for a South Pole ($\varphi \leq -60^\circ$). In (Chabot et al. 2018) showed that the area of permanently shadowed regions in the South polar regions of the Mercury for $\varphi \geq 80^\circ$ S is 5.7% of this region’s surface area, and in the north regions, it is 3.7% of polar regions area. These data are consistent with our estimations; according to them, the fractions of permanently shadowed areas of the surface in these regions ($\varphi \geq 80^\circ$ S) are 5.9% and 3.4%. The obtained values of permanently shadowed regions’ area allowed us to evaluate the fraction of water molecules that fall into these regions. From the moment when a particle gets in a permanently shadowed area, it was considered as a molecule that stays there forever and was not included in the further modeling.

Overall, modeling in this research included 2000 000 particles (water molecules). According to the obtained results, nearly 0.27% of water molecules will leave the planet’s exosphere as a result of their escape velocity’s (Fig. 3) threshold value for Mercury—4251 m/s.

We found that most of the molecules involved in the modeling—about 91.93% on average—will be destroyed as a result of photolysis. Of these, about 7.46% will be

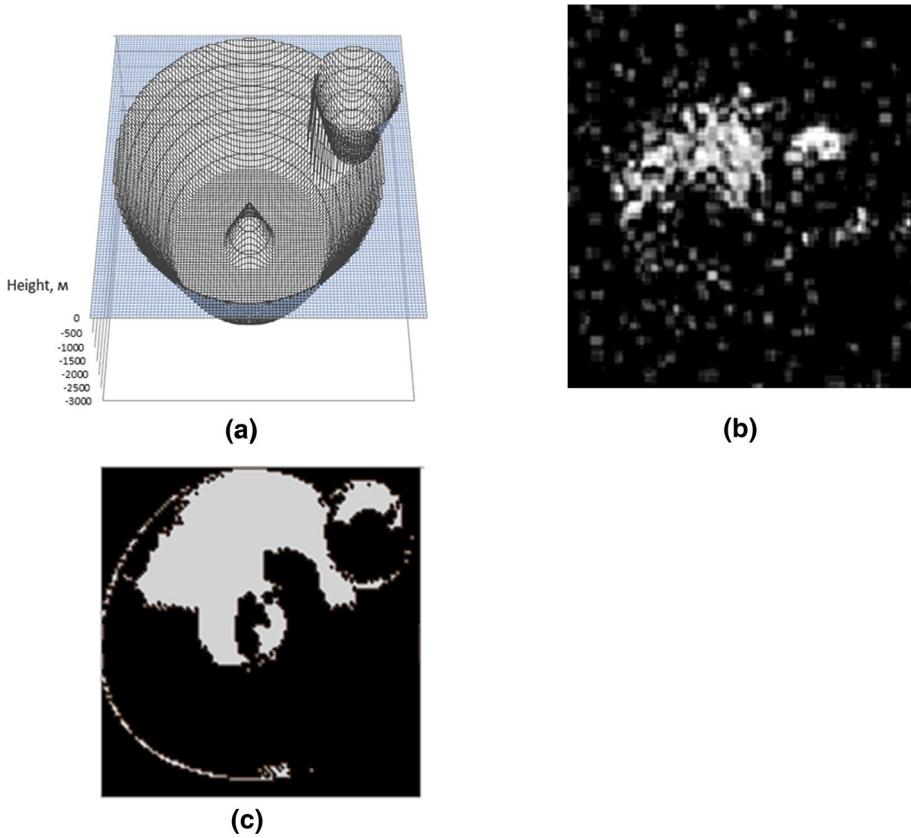


Fig. 2 **a** The model of the inner shape of Hurley crater (87.4° S, 7° W) with a satellite crater on the slope; **b** the image of radar-bright feature U in the Hurley crater (Chabot et al. 2018); **c** the distribution of permanently shadowed areas of crater Hurley according to our data

Table 1 The distribution of constantly shadowed regions that are located inside of impact craters in the Mercury’s polar regions ($|\varphi| \geq 60^\circ$)

Latitude Region	Fraction of surface, %	Area, km ²
$60^\circ \leq \varphi \leq 70^\circ$	0.003	92.4
$70^\circ < \varphi \leq 80^\circ$	0.24	3964
$80^\circ < \varphi \leq 90^\circ$	3.4	19,211
$-60^\circ \geq \varphi \geq -70^\circ$	0.008	219.6
$-70^\circ \geq \varphi \geq -80^\circ$	0.7	11,711
$-80^\circ \geq \varphi \geq -90^\circ$	5.9	33,568

destroyed as a result of photolysis while on the planet’s surface. The fraction of molecules destroyed as a result of photolysis in flight depends on the starting latitude of the molecules. Its value ranges from 60% for molecules that started at high latitudes ($|\varphi| \geq 80^\circ$) to almost 90% for molecules that started at the equator and in middle latitudes ($|\varphi| \leq 60^\circ$). According to our estimates, about 7.8% of the total number of water

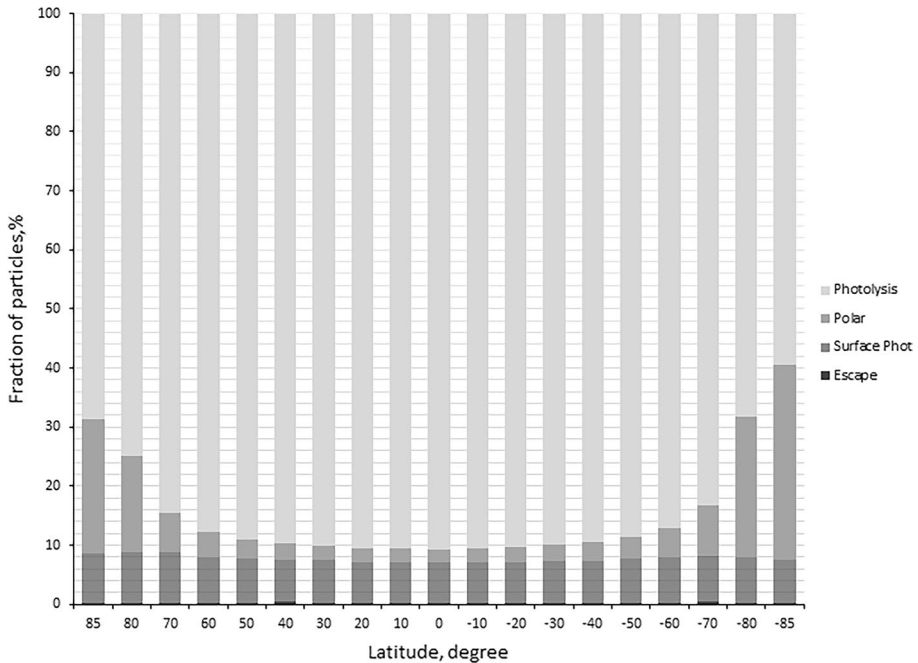


Fig. 3 Distribution of particles by processes depending on the starting latitude of the launch site. The total number of particles participating in the simulation ($2 \cdot 10^6$) is taken as 100%

molecules will fall into the constantly shaded areas of the planet's polar regions. This result is consistent with the estimate of the proportion of molecules falling into permanently shaded regions in the polar regions of Mercury, obtained in (Butler 1997): 5–15%. The constantly shaded areas in the northern polar region of the planet will receive almost 2 times less water molecules than in the southern: 2.2 and 5.6% of the total, respectively.

Figure 4 shows the distribution of the proportion of molecules trapped in permanently shaded regions depending on the starting latitude. As can be seen from Fig. 4, the largest contribution to the deposits in the permanently shaded areas of the polar regions of the planet is made by particles whose launch site is located at latitudes $|\varphi| \geq 70^\circ$. Only 0.6% of the total number of particles launched in the equatorial ($-10^\circ \leq \varphi \leq 10^\circ$) zone of the planet will fall into permanently shaded areas near the North Pole and 1.6% at the South Pole.

A number of studies investigated the fraction of impactor matter retained in the exosphere during collisions of asteroids and comets with the surface of Mercury. According to (Syal and Schultz, 2015a), if the velocity of collision of a body with Mercury is 15 km/s, then the fraction of the projectile material retained during such a collision reaches 100%. This value reaches 0% at a collision velocity of 60 km/s (Syal and Schultz 2015b). The fraction of the conserved comet matter at collision velocities of 15 and 30 km/s reaches 28 and 16%, respectively (Syal and Schultz 2015b). It was shown in (Le Feuvre and Wicczorek, 2008) that asteroids can be a more significant source of water on Mercury, since already at a collision speed of 45 km / s, the fraction of the

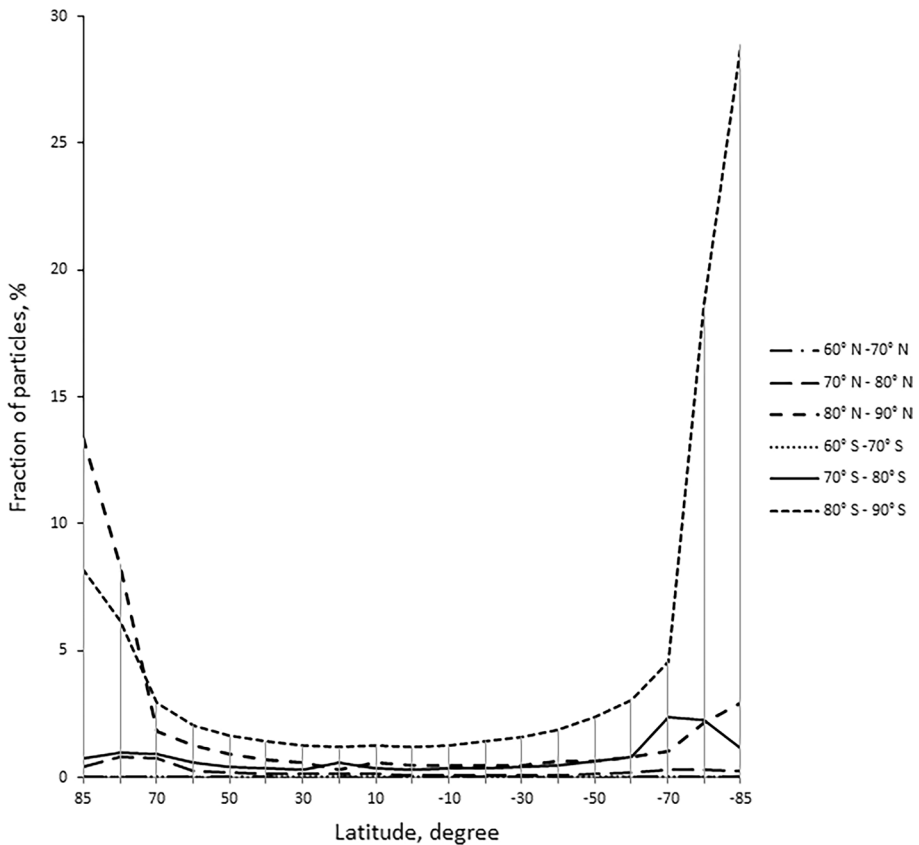


Fig. 4 The proportion of particles trapped in the permanently shaded areas in the polar regions of Mercury, depending on the starting latitude of molecules. The total number of molecules participating in the simulation ($2 * 10^6$) is taken as 100%

comet's stored matter falls to 0. The average collision speed for Mercury is 42.5 km/s (Le Feuvre and Wieczorek, 2008). Similar estimates are given in (Ernst et al. 2018): at a collision speed of 10 km/s, 100% of the comet matter is retained, and at a collision speed of 80 km/s, only 0.4% of the comet matter.

The water content in asteroids ranges from 5 (Moses et al. 1999) to 20% (carbonaceous chondrites). The fraction of water in the comet structure is 50–70%. The values of comet density can fluctuate from 0.4 g/cm^3 for Churyumov-Gerasimenko comet (Baldwin 2014) to 1.2 g/cm^3 (Ong et al. 2010). The comet sizes can fluctuate from 1 to 20 km in diameter. When an asteroid collides with the size of 5 m to 5 km with the surface of Mercury, from $1.3 * 10^6$ to $1.3 * 10^{16}$ g of water can be saved. When a comet from 1 to 20 km in size falls on the surface of Mercury, from 10^{12} to $3 * 10^{18}$ g of water can be preserved in cold traps in the both polar regions. Our estimates of the amount of water entering permanently shaded regions in the polar regions of Mercury as a result of such collisions are given in Table 2. Currently, the reserves of water ice in the cold traps of the polar regions of the planet are estimated at 10^{16} – 10^{18} g (Ernst et al. 2018). This amount of water can be obtained as a result of collisions with the planet's surface of several dozen asteroids and comets. The

Table 2 The maximum and minimum amount of water delivered to permanently shaded areas around the North and South poles of Mercury as a result of a single collision, depending on the source of origin

	North Pole		South Pole	
	Minimum	Maximum	Minimum	Maximum
Asteroids	$2.4 * 10^4$ g	$2.9 * 10^{14}$ g	$6 * 10^4$ g	$7.3 * 10^{14}$ g
Comets	$2.3 * 10^{10}$ g	$6.5 * 10^{16}$ g	$6 * 10^{10}$ g	$1.6 * 10^{17}$ g

probability of collision of an asteroid or comet with the surface of Mercury was estimated in (Moses et al. 1999). For comets, the average value of this value is $4.28 * 10^{-10}$ per year, for asteroids— $2.74 * 10^{-9}$ per year. In this case, in 1 million years, from tens to $2 * 10^{12}$ g of water can be delivered to the polar regions of the planet as a result of falling asteroids and from 10^7 to $7 * 10^{13}$ g of water as a result of falling comets.

6 Conclusions

We have simulated the migration of water molecules in the exosphere of Mercury, delivered as a result of collisions of comets and asteroids with the planet's surface.

To estimate the proportion of water molecules falling into cold traps in the polar regions of Mercury, we estimated the area of such regions. For this, the model of the structure of Mercury craters developed by Pike (1988) was used. We found that the area of permanently shaded areas near the north pole of the planet reaches $23,300 \text{ km}^2$, and in the area of the south pole— $45,500 \text{ km}^2$.

According to our results, most of the water molecules ($\sim 92\%$) will be destroyed by photolysis, including 7.46% that will be destroyed while on the planet's surface between jumps. The proportion of water molecules that left the exosphere of the planet as a result of reaching the cosmic speed is only 0.3%.

The fraction of water molecules trapped in permanently shaded areas in the polar regions of Mercury reaches 7.8% of the total number of particles participating in the simulation. Only 2.2% of them can be trapped in cold traps in the North Pole region and 5.6% in the South Pole region.

Acknowledgements This research was supported by Russian Foundation for Basic Research (RFBR), project No 20-35-70019 "Creation of global catalog of Mercury craters for fundamental planetary research".

References:

- E. Baldwin, "Measuring Comet 67P/C-G". European Space Agency. Retrieved 16 November, 2014
- K.J. Becker, M.S. Robinson, T.L. Becker, L.A. Weller, K.L. Edmundson, G.A. Neumann, M.E. Perry, S.C. Solomon, Book of proceeding 47th Lunar and Planetary conference, Abstract # 1903 (2016)
- B.J. Butler, *J. Geophys. Res* **102**, 19283–19291 (1997)
- P.K. Byrne, C.I. Fassett, C. Klimczak, L.R. Ostrach, C.R. Chapman, B.W. Denevi, A. M. Celâl Şengör, S. A. Hauck, A.J. Evans, M.E. Banks, T.R. Watters, J.W. Head, and S.C. Solomon, Book of proceeding 47th Lunar and Planetary conference, Abstract # 1227 (2016)
- N.L. Chabot, E.E. Shread, J.K. Harmon, *J. Geophys. Res* (2018). <https://doi.org/10.1002/2017JE005500>
- A. Colaprete, P. Schultz, J. Heldmann, D. Wooden, M. Shirley, K. Ennico, *Sci.* (2010). <https://doi.org/10.1016/j.pss.2008.06.019C.M>

- N.L. Ernst, O.S. Chabot, Barnouin. *JGR* **123**, 2628–2646 (2018)
- G. Cremonese, J. Warell, J.K. Harmon, F. Leblanc, M. Mendillo, A.L. Sprague, *Planet. Space Sci.* **58**, 61–78 (2010)
- B. Fegley, *GRL* **18**, 2073–2076 (1991)
- E.A. Feoktistova, A.Yu. Zharkova, A.A. Kokhanov, Zh.F. Rodionova, V.A. Rotaru. Book of proceeding 11th Moscow Solar System Symposium (11M-S 3), (2020)
- G.R. Gladstone, D.M. Hurley, K.D. Retherford, P.D. Feldman, W.R. Pryor, J.-Y. Chaufray, M. Versteeg, T.K. Greathouse, A.J. Steffl, H. Throop, J.W. Parker, D.E. Kaufmann, A.F. Egan, M.W. Davis, D.C. Slater, J. Mukherjee, P.F. Miles, A.R. Hendrix, A. Colaprete, S.A. Stren, *Sci.* **58**(1–2), 61–78 (2010). <https://doi.org/10.1016/j.pss.2008.06.019>
- A. Grumpe, Ch. Wohler, A.A. Berezhnoy, V.V. Shevchenko, *Icarus* (2019). <https://doi.org/10.1016/j.icarus.2018.11.025J>
- J.K. Harmon, M.A. Slade, *Sci.* **258**, 640–643 (1992)
- J.K. Harmon, P.J. Perillat, *Icarus* **149**, 1–15 (2001)
- J.K. Harmon, M.A. Slade, M.S. Rice, *Icarus* **211**, 37–50 (2011). <https://doi.org/10.1016/j.icarus.2010.08.007>
- W.F. Huebner, J.J. Keady, S.P. Lyon, *Ast. Space Sci.* **195**, 1–294 (1992)
- M. Le Feuvre, M.A. Wieczorek, *Icarus* **197**(1), 291–306 (2008). <https://doi.org/10.1016/j.icarus.2008.04>
- J.E. Moores, *J. Geophys. Res.* **121**, 46–60 (2015). <https://doi.org/10.1002/2015JE004929>
- J.I. Moses, K. Rawlins, K. Zahnle, L. Dones, *Icarus* **137**, 197–221 (1999)
- G.A. Neumann, J.F. Cavanaugh, X. Sun, E.M. Mazarico, D.E. Smith, M.T. Zuber, *Sci.* (2013). <https://doi.org/10.1126/science.1229764>
- D. Nesvorny, P. Jenniskens, H.F. Levison, W.F. Bottke, D. Vokrouhlicky, M. Gounelle, *Astrophys. J.* **713**, 816–836 (2010)
- L. Ong, E.I. Asphaug, D. Korycansky, R.F. Coker, *Icarus* **207**, 578–589 (2010). <https://doi.org/10.1016/j.icarus.2009.12.012>
- D.A. Paige, M.A. Siegler, J.K. Harmon, G.A. Neumann, E.M. Mazarico, D.E. Smith, M.T. Zuber, E. Harju, M.L. Delitsky, S.C. Solomon, *Science* (2012). <https://doi.org/10.1126/science.1231106>
- E. Pierazzo, C.F. Chyba, *Meteorit. Planet. Sci.* **34**, 909–918 (1999)
- P.J. Pike (1988) In *Mercury*, By F. Vilas, C. R. Chapman, and M. S. Matthews, Eds. (Univ. of Arizona Press, Tucson, 1988), pp. 165–273
- P. Prem, N.A. Artemieva, D.B. Goldstein, P.L. Varghese, L.M. Trafton, *Icarus* **255**, 148–158 (2015)
- N. Schorghofer, *Phys. Rev. e.* **91**, 052154 (2015)
- M.B. Syal, P.H. Schultz, *Icarus* **257**, 194–206 (2015)
- M. B. Syal and P. H. Schultz, Book of proceeding 47th Lunar and Planetary conference (LPSC), Abstract # 1680 (2015)
- R.J. Thomas, D.A. Rothery, S.J. Conway, M. Anand, *Geophys. Res. Lett.* **41**(17), 6084–6092 (2014)
- A.R. Vasavada, D.A. Paige, S.E. Wood, *Icarus* **141**, 179–193 (1999)
- P. Wurz, H. Lammer, *Icarus* **164**, 1–13 (2003). [https://doi.org/10.1016/S0019-1035\(03\)00123-4](https://doi.org/10.1016/S0019-1035(03)00123-4)
- J.A. Zhang, D.A. Paige, *GRL* (2009). <https://doi.org/10.1029/2009GL038614>
- B.M. Jones, M. Sarantos, T.M. Orlando, *ApJL* (2020). <https://doi.org/10.3847/2041-8213/ab6bda>
- D.J. Lawrence, W.C. Feldman, J.O. Goldsten, S. Maurice, P.N. Peplowski, B.J. Anderson, D. Bazell, R.L.J.R. McNutt, L.R. Nittler, P.N. Prettyman, D.J. Rogers, S.C. Solomon, S.Z. Weider, *Sci.* **339**, 292–296 (2013). <https://doi.org/10.1126/science.1229953>
- B.D. Sitnikov, E.A. Kozlova, J.F. Rodionova, Book of proceeding 22d International Cartographic Conference (ICC) (2005)